Sensors and Materials, Vol. 38, No. 2 (2026) 747–752
MYU Tokyo

S & M 4344

Performance of Eu^{3+}-doped Garnet Scintillator–Silicon Photodiode Systems for Nuclear Photovoltaic Battery Applications

Toshiaki Kunikata,[1*] Kai Okazaki,[1] Hiromi Kimura,[2] Yuta Tominaga,[1,3]
Takumi Kato,[1] Daisuke Nakauchi,[1] Noriaki Kawaguchi,[1] and Takayuki Yanagida[1]

[1]Nara Institute of Science and Technology, 8916-5 Takayama, Ikoma, Nara 630-0192, Japan
[2]National Institute of Advanced Industrial Science and Technology,
1-1-1 Umezono, Tsukuba, Ibaraki 305-8568, Japan
[3]Electrical Engineering, Fukuoka University, Nanakuma, Fukuoka, Japan

(Received October 31, 2025; accepted December 19, 2025)

Keywords: nuclear battery, scintillation, garnet single crystal

The X-ray-induced power generation characteristics of Eu^{3+}-doped $Y_3Al_5O_{12}$ (YAG), $Gd_3Al_2Ga_3O_{12}$ (GAGG), and $Lu_3Al_5O_{12}$ (LuAG) single crystal scintillators with different Eu concentrations were evaluated. The generated electrical power densities were then compared with the scintillation light yields and the integrated intensities of scintillation spectra in the 550–690 nm range. Although the LuAG:Eu samples exhibited lower light yields than the YAG:Eu and GAGG:Eu samples, they showed comparable or higher generated power densities owing to their higher effective atomic number (Z_{eff} = 64), which enhances photoelectric absorption efficiency. A good correlation was observed between the power densities and the integrated intensities of scintillation spectra, whereas the relationship between the light yields and integrated intensities was less significant owing to the influence of afterglow and variations in photoelectric absorption.

1. Introduction

Radiation detectors are widely used in various fields such as medical,[1–6] industrial, well-logging,[7] environmental monitoring,[8] and security[9–12] applications. Some of these radiation detectors utilize scintillators, which are a type of phosphor material that instantly converts high-energy ionizing radiation into numerous low-energy visible or near-visible photons.[13] The essential characteristics required for scintillators include a high light yield, chemical stability, a suitable effective atomic number (Z_{eff}), and high density. Because these properties must be optimized for different purposes, scintillators have been developed in various material forms such as nanoparticles,[14–16] crystals,[17–23] ceramics,[21,24–26] and glasses.[27–32]

In recent years, scintillator-based devices have attracted considerably increasing attention for potential applications beyond conventional radiation detection. One emerging concept is the use of scintillators as energy converters in nuclear photovoltaic batteries,[25,33–36] where the radiative

*Corresponding author: e-mail: kunikata.toshiaki.kt1@ms.naist.jp
https://doi.org/10.18494/SAM6034

ISSN 0914-4935
https://myukk.org/

energy emitted by radioisotopes is transformed into electrical energy through the combination of a scintillator and a photovoltaic device such as a silicon photodiode (Si-PD). This scintillator–photodiode approach is considered promising for large-scale applications, including auxiliary power generation in nuclear power facilities. In such systems, the performance strongly depends on the light yield and emission spectra of the scintillators, as well as its spectral matching with the photodiode's sensitivity range. To optimize this interaction, the selection of activator ions with suitable emission characteristics is essential.

Among various luminescent ions, Eu^{3+} ions have been considered a promising activator because they exhibit 4f–4f emission peaks in the long-wavelength red region, which better overlaps with the higher sensitivity range of Si-PD than the luminescence from other dopants such as Ce^{3+} ions. Therefore, Eu^{3+} ions are advantageous for enhancing photovoltaic conversion efficiency in scintillator–photodiode systems. Furthermore, Eu^{3+}-activated oxide-based scintillators such as $Y_3Al_5O_{12}$ (YAG),[37] $Gd_3Al_2Ga_3O_{12}$ (GAGG),[38] and $Lu_3Al_5O_{12}$ (LuAG)[39] exhibit high light yields and excellent chemical stability, mechanical strength, and optical transparency, making them potential candidates for durable nuclear battery materials. Regarding the spectral characteristics, although slight differences in the relative peak intensities of 4f–4f transitions of Eu^{3+} ions exist among garnet hosts, the overall spectral shapes are similar.[37–39] Thus, the effects of spectral variations are reduced, allowing a fair comparison of other properties among the samples under identical spectral conditions.

In this study, the performances of YAG:Eu^{3+}, GAGG:Eu^{3+}, and LuAG:Eu^{3+} single crystals were evaluated in combination with a Si-PD under X-ray excitation. The relationships among the generated electrical power densities, scintillation light yields, and the integrated intensities of the scintillation spectra were investigated.

2. Materials and Methods

Eu-doped $Y_{3(1-x)}Al_5O_{12}$, $Gd_{3(1-x)}Al_2Ga_3O_{12}$, and $Lu_{3(1-x)}Al_5O_{12}$ single crystals with different Eu concentrations (x = 0.005, 0.01, 0.05, 0.1, and 0.15 corresponding to 0.5, 1.0, 5.0, 10.0, and 15.0%) reported in previous studies were used in this work.[37–39] These single crystals were grown by the floating zone method, followed by mechanical processing and optical polishing.

Power densities generated from the combination of Eu^{3+}-doped garnet single crystals and Si-PD under X-ray irradiation were evaluated for nuclear photovoltaic battery applications using a custom-made setup. A schematic diagram of the experimental setup is presented in Fig. 1. The scintillator was optically coupled to an optical fiber (UD0065, Asahi Spectra), which in turn was connected to a Si-PD (Hamamatsu, S12915-66R). Scintillation photons generated within the samples were transmitted through the fiber and subsequently detected by the Si-PD. This configuration ensured a sufficient distance between the photodiode and the X-ray source, thereby preventing the direct irradiation of the Si-PD. To further reduce unwanted exposure, the Si-PD was enclosed by a 3-mm-thick lead shielding to suppress scattered X-rays. The electrical signal from the Si-PD was monitored using a picoammeter (Keysight B2985A) with an integration time of 0.3 s. The photocurrents from the samples were measured using the picoammeter, and the power densities were calculated from the measured currents and an open-

circuit voltage of the Si-PD (0.45 V).[40] An X-ray generator operated at 40 kV and 1.2 mA was used as the radiation source.

After calculating the generated power densities for the samples, the correlations among the power densities, scintillation light yields, and the integrated intensities of scintillation spectra of the samples were evaluated. The measurement time was 1 min. The integrated intensities of scintillation spectra under X-ray irradiation were measured using an original optical measurement system.[41] The excitation source was an X-ray generator (XRB80P & N200X4550, Spellman). The scintillation light from the samples was transmitted to a CCD spectrometer (DU-420-BU2, Andor) through an optical fiber, and the integrated intensities between 550 and 690 nm were recorded. In this measurement, the tube voltage and current of the X-ray generator were set to 40 kV and 1.2 mA, respectively.

The light yields were estimated on the basis of previously reported pulse height spectra under γ-ray irradiation from ^{137}Cs (662 keV).[37–39] To calculate the light yields correctly, the quantum efficiency (*QE*) of a photomultiplier tube of the reference scintillator $Bi_4Ge_3O_{12}$ (BGO)[42] was assumed to be 16.7%, and the *QE* of the Eu-doped garnet samples was assumed to be 13.6 %.

3. Results and Discussion

Figure 2 shows the correlation between the generated power densities and the scintillation light yields of the samples. LuAG:Eu samples exhibited comparable or even higher power densities than YAG:Eu and GAGG:Eu samples, despite their lower light yields. This can be attributed to the relatively high effective atomic number of LuAG (Z_{eff} = 64), which results in a higher probability of photoelectric absorption of X-rays than those of YAG (Z_{eff} = 32) and GAGG (Z_{eff} = 54). Additionally, LuAG:Eu (5.0%) exhibited the highest power density (around 190 nW/cm^3) among all the samples.

Figure 3 indicates the relationship between the generated power densities and the integrated intensities of scintillation spectra under X-ray irradiation. Overall, a better correlation was observed between the power densities and the integrated intensities than that shown in Fig. 2.

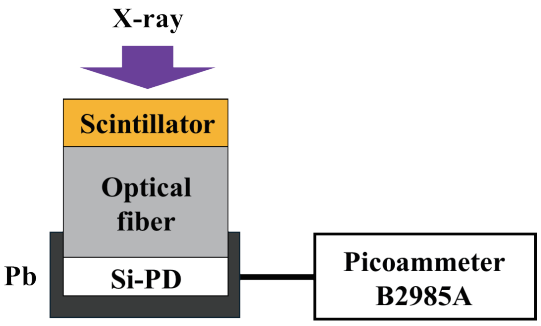

Fig. 1. (Color online) Schematic of the experimental setup used.

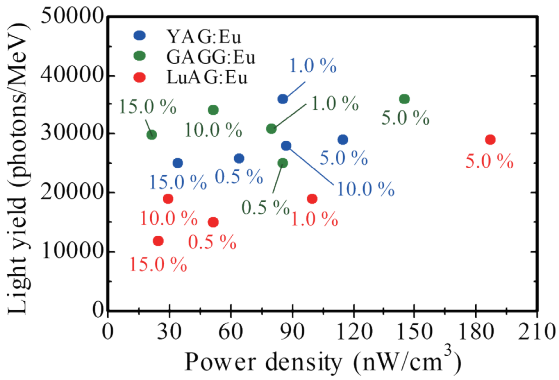

Fig. 2. (Color online) Relationship between generated power densities and light yields.

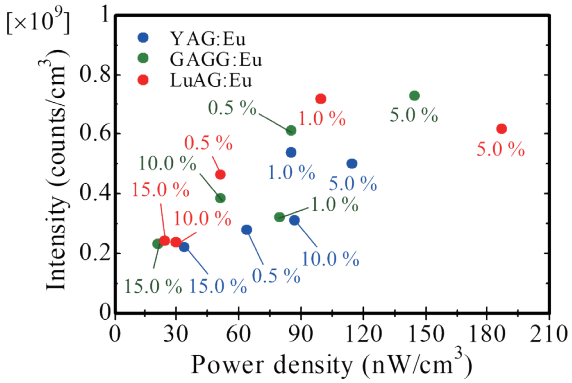

Fig. 3. (Color online) Relationship between generated power densities and scintillation intensities.

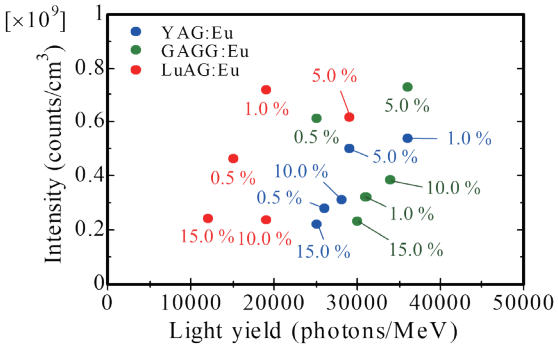

Fig. 4. (Color online) Relationship between light yields and scintillation intensities.

This is likely because the scintillation, afterglow components, and Z_{eff} of the samples contributed in a similar manner in these measurements. Because both the power densities and the integrated intensities were obtained using integration-based detection methods under X-ray irradiation, these factors were consistently reflected, resulting in more systematic data. On the other hand, the integrated intensities were measured with an integration time of 1 min, whereas the generated power densities were measured with a shorter integration time of 0.3 s. Owing to this difference, spectral measurements are more susceptible to afterglow contributions, while the shorter integration time might reduce the influence of afterglow in the power-density evaluation.

The correlation between the light yields and the integrated intensities of the samples is shown in Fig. 4. In general, the correlation between these two parameters was not particularly strong. This can be attributed to the fact that the integrated intensities are affected by not only the light yields but also the afterglow components and the photoelectric absorption efficiencies. Therefore, multiple parameters are considered to have influenced the overall correlation. These results demonstrate that the integrated intensities provide a practical parameter for evaluating the energy conversion performance in scintillator–photodiode systems.

4. Conclusions

The energy conversion characteristics of Eu^{3+}-activated YAG, GAGG, and LuAG single crystals coupled with a Si-PD were investigated under X-ray excitation. Among the examined samples, the 5.0% LuAG:Eu^{3+} sample exhibited the highest generated power density (approximately 190 nW/cm³). This result is mainly attributed to the higher effective atomic number of LuAG, which enhances X-ray absorption and thereby increases the overall conversion efficiency. A good correlation was observed between the generated power densities and the integrated intensities, whereas the relationship with the light yields was weaker, likely because of the influence of afterglow and variations in photoelectric absorption.

Acknowledgments

This work was supported by JSPS Fellows for Young Scientists (24KJ1693 and 23KJ1592) from the Japan Society for the Promotion of Science, Research Foundation for the Electrotechnology of Chubu, Shimadzu Science Foundation, and the Cooperative Research Project of the Research Center for Biomedical Engineering.

References

1 I. Kandarakis, D. Cavouras, E. Kanellopoulos, C. D. Nomicos, and G. S. Panayiotakis: Radiat. Meas. **29** (1998) 481. https://doi.org/10.1016/S1350-4487(98)00058-4
2 C. Ronda, H. Wieczorek, V. Khanin, and P. Rodnyi: ECS J. Solid State Sci. Technol. **5** (2016) R3121. https://doi.org/10.1149/2.0131601jss
3 I. Kandarakis, D. Cavouras, I. Sianoudis, D. Nikolopoulos, A. Episkopakis, D. Linardatos, D. Margetis, E. Nirgianaki, M. Roussou, P. Melissaropoulos, N. Kalivas, I. Kalatzis, K. Kourkoutas, N. Dimitropoulos, A. Louizi, C. Nomicos, and G. Panayiotakis: Nucl. Instrum. Methods Phys. Res. A **538** (2005) 615. https://doi.org/10.1016/j.nima.2004.08.101
4 C. W. E. van Eijk: Nucl. Instrum. Methods Phys. Res. A **509** (2003) 17. https://doi.org/10.1016/S0168-9002(03)01542-0
5 K. Tanderup, S. Beddar, C. E. Andersen, G. Kertzscher, and J. E. Cygler: Med. Phys. **40** (2013) 070902. https://doi.org/10.1118/1.4810943
6 S. David, M. Georgiou, E. Fysikopoulos, and G. Loudos: Phys. Medica **31** (2015) 763. https://doi.org/10.1016/j.ejmp.2015.03.008
7 C. L. Melcher: Nucl. Inst. Methods Phys. Res. B **40–41** (1989) 1214. https://doi.org/10.1016/0168-583X(89)90622-8
8 K. Watanabe, T. Yanagida, K. Fukuda, A. Koike, T. Aoki, and A. Uritani: Sens. Mater. **27** (2015) 269. https://doi.org/10.18494/SAM.2015.1093
9 L. E. Sinclair, D. S. Hanna, A. M. L. MacLeod, and P. R. B. Saull: IEEE Trans. Nucl. Sci. **56** (2009) 1262. https://doi.org/10.1109/TNS.2009.2019271
10 V. D. Ryzhikov, A. D. Opolonin, P. V. Pashko, V. M. Svishch, V. G. Volkov, E. K. Lysetskaya, D. N. Kozin, and C. Smith: Nucl. Instrum. Methods Phys. Res. A **537** (2005) 424. https://doi.org/10.1016/j.nima.2004.08.056
11 J. Glodo, Y. Wang, R. Shawgo, C. Brecher, R. H. Hawrami, J. Tower, and K. S. Shah: Phys. Procedia **90** (2017) 285. https://doi.org/10.1016/j.phpro.2017.09.012
12 Q. Liu, Y. Cheng, Y. Yang, Y. Peng, H. Li, Y. Xiong, and T. Zhu: Appl. Radiat. Isot. **163** (2020) 109217. https://doi.org/10.1016/j.apradiso.2020.109217
13 T. Yanagida: Proc. Japan Acad. Ser. B **94** (2018) 75. https://doi.org/10.2183/pjab.94.007
14 M. Koshimizu, K. Tanahashi, Y. Fujimoto, and K. Asai: Sens. Mater. **37** (2025) 539. https://doi.org/10.18494/SAM5448
15 M. Koshimizu, Y. Fujimoto, and K. Asai: Sens. Mater. **35** (2023) 521. https://doi.org/10.18494/SAM4149
16 L. Sudheendra, G. K. Das, C. Li, D. Stark, J. Cena, S. Cherry, and I. M. Kennedy: Chem. Mater. **26** (2014) 1881. https://doi.org/10.1021/cm404044n
17 M. Ishida, A. Watanabe, H. Kawamoto, Y. Fujimoto, and K. Asai: Sens. Mater. **37** (2025) 607. https://doi.org/10.18494/SAM5482
18 Y. Fujimoto, and K. Asai: Jpn. J. Appl. Phys. **62** (2023) 010605. https://doi.org/10.35848/1347-4065/ac9348
19 A. Ito and S. Matsumoto: Jpn. J. Appl. Phys. **62** (2023) 010612. https://doi.org/10.35848/1347-4065/aca249
20 M. Koshimizu: Jpn. J. Appl. Phys. **62** (2023) 010503 . https://doi.org/10.35848/1347-4065/ac94fe
21 S. Otake, S. Takase, T. Kato, D. Nakauchi, N. Kawaguchi, and T. Yanagida: Sens. Mater. **37** (2025) 519. https://doi.org/10.18494/SAM5433
22 Y. Endo, K. Ichiba, and D. Nakauchi: Sens. Mater. **37** (2025) 587. https://doi.org/10.18494/SAM5432
23 S. Matsumoto, T. Watanabe, and A. Ito: Sens. Mater. **34** (2022) 669. https://doi.org/10.18494/SAM3698
24 Y. Shao, R. L. Conner, N. R. S. Souza, R. S. Silva, and L. G. Jacobsohn: Jpn. J. Appl. Phys. **62** (2023) 010601. https://doi.org/10.35848/1347-4065/ac9941
25 Y. Zhuang, Z. Luo, R. Lu, H. Tang, T. Zhang, Y. Liu, P. Sun, and J. Jiang: Appl. Mater. Today **43** (2025) 102625. https://doi.org/10.1016/j.apmt.2025.102625

26 T. Kato, D. Nakauchi, N. Kawaguchi, and T. Yanagida: Sens. Mater. **36** (2024) 531. https://doi.org/10.18494/SAM4749
27 N. Wantana, E. Kaewnuam, Y. Tariwong, N. D. Quang, P. Pakawanit, C. Phoovasawat, N. Vittayakorn, S. Kothan, H. J. Kim, and J. Kaewkhao: Jpn. J. Appl. Phys. **62** (2023) 010602. https://doi.org/10.35848/1347-4065/ac9876
28 H. Fukushima, R. Tsubouchi, T. Matsuura, T. Yoneda, and T. Yanagida: Sens. Mater. **37** (2025) 487. https://doi.org/10.18494/SAM5438
29 S. Muneta, N. Kawano, D. Nakauchi, T. Kato, K. Okazaki, K. Ichiba, T. Kunikata, A. Nishikawa, K. Miyazaki, F. Kagaya, K. Shinozaki, and T. Yanagida: Sens. Mater. **37** (2025) 509. https://doi.org/10.18494/SAM5441
30 K. Miyajima, A. Nishikawa, T. Kato, D. Nakauchi, N. Kawaguchi, and T. Yanagida: Sens. Mater. **37** (2025) 481. https://doi.org/10.18494/SAM5436
31 Y. Oshima, K. Watanabe, H. Shiga, and G. Wakabayashi: Sens. Mater. **35** (2023) 545. https://doi.org/10.18494/SAM4148
32 D. Shiratori, H. Fukushima, D. Nakauchi, T. Kato, N. Kawaguchi, and T. Yanagida: Jpn. J. Appl. Phys. **62** (2023) 010608. https://doi.org/10.35848/1347-4065/ac90a4
33 L. Hong, X. Bin Tang, Z. H. Xu, Y. P. Liu, and D. Chen: Nucl. Inst. Methods Phys. Res. B **338** (2014) 112. https://doi.org/10.1016/j.nimb.2014.08.005
34 Z. Zhang, X. Tang, Y. Liu, Z. Xu, H. Ye, F. Tian, K. Liu, Z. Yuan, and W. Chen: Sens. Actuators, A **290** (2019) 162. https://doi.org/10.1016/j.sna.2019.03.024
35 Q. Cui, J. Lu, X. Li, X. Yuan, Y. Zhao, R. Zheng, Q. Li, J. Wei, B. Luo, and L. Lin: Mater. Sci. Semicond. Process. **179** (2024) 108493. https://doi.org/10.1016/j.mssp.2024.108493
36 T. Yanagida, K. Okazaki, K. Miyajima, T. Kato, D. Nakauchi, and N. Kawaguchi: Sens. Mater. **37** (2025) 453. https://doi.org/10.18494/SAM5423
37 T. Kunikata, K. Watanabe, P. Kantuptim, D. Shiratori, T. Kato, D. Nakauchi, N. Kawaguchi, and T. Yanagida: Radiat. Phys. Chem. **216** (2024) 111454. https://doi.org/10.1016/j.radphyschem.2023.111454
38 T. Kunikata, K. Watanabe, P. Kantuptim, K. Ichiba, D. Shiratori, T. Kato, D. Nakauchi, N. Kawaguchi, and T. Yanagida: Jpn. J. Appl. Phys. **63** (2024) 01SP18. https://doi.org/10.35848/1347-4065/acfb16
39 T. Kunikata, K. Watanabe, H. Kimura, K. Okazaki, T. Kato, D. Nakauchi, N. Kawaguchi, and T. Yanagida: Solid State Sci. **163** (2025) 107902. https://doi.org/10.1016/j.solidstatesciences.2025.107902
40 T. Yanagida, K. Miyajima, K. Okazaki, Y. Tominaga, T. Kato, D. Nakauchi, and N. Kawaguchi: Sens. Mater. **38** (2026) 753. https://doi.org/10.18494/SAM6003
41 T. Yanagida, K. Kamada, Y. Fujimoto, H. Yagi, and T. Yanagitani: Opt. Mater. **35** (2013) 2480. https://doi.org/10.1016/j.optmat.2013.07.002
42 I. Holl, E. Loren, and G. Mageras: IEEE Trans. Nucl. Sci. **35** (1988) 105. https://doi.org/10.1109/23.12684